Acta Pharm. 56 (2006) 157–174 Original research paper

3D-QSAR CoMFA/CoMSIA studies on 5-aryl-2,2-dialkyl--4-phenyl-3(2*H*)-furanone derivatives, as selective COX-2 inhibitors

DEVENDRA SHARAD PUNTAMBEKAR
RAJANI GIRIDHAR
MANGE RAM YADAV*

Pharmacy Department
Faculty of Technology and Engineering, Kalabhavan

The M. S. University of Baroda
Vadodara-390001, India

Comparative Molecular Field Analysis (CoMFA) and Comparative Molecular Similarity Indices Analysis (CoMSIA) were performed on a series of 5-aryl-2,2-dialkyl-4-phenyl--3(2*H*)-furanone derivatives, as selective cyclooxygenase--2 (COX-2) inhibitors. Ligand molecular superimposition on the template structure was performed by the atom/shape based root mean square fit and database alignment methods. Removal of three outliers from the initial training set of 49 molecules improved the predictivity of the model. The statistically significant model was established of 36 molecules, which were validated by a test set of ten compounds. The atom and shape based root mean square alignment (IV) yielded the best predictive CoMFA model [R^2_{cv} = 0.664, R^2 (non-cross-validated square of correlation coefficient) = 0.916, F value = 47.341, R^2_{bs} = 0.947 with six components, standard error of prediction$_{36}$ = 0.360 and standard error of estimate$_{36}$ = 0.180] while the CoMSIA model yielded [R^2_{cv} = 0.777, R^2 (non-cross--validated square of correlation coefficient) = 0.905, F value = 66.322, R^2_{bs} = 0.933 with four components, standard error of prediction$_{36}$ = 0.282 and standard error of estimate$_{36}$ = 0.185]. The contour maps obtained from 3D--QSAR studies were appraised for activity trends for the molecules analyzed. Results indicate that steric, electrostatic, hydrophobic (lipophilic) and hydrogen bond donor substituents play a significant role in COX-2 inhibitory activity and selectivity of the compounds. The data generated from the present study will further help design novel, potent and selective COX-2 inhibitors.

Keywords: 3D-QSAR, CoMFA, CoMSIA, cyclooxygenase--2 inhibitors, anti-inflammatory agents

Accepted December 4, 2005

* Correspondence, e-mail: mryadav@sify.com

Nonsteroidal anti-inflammatory drugs (NSAIDs) are widely used to alleviate the symptoms of inflammatory diseases (1, 2). The principal pharmacological effects of NSAIDs are due to their ability to inhibit prostaglandin synthesis by blocking cyclooxygenase (COX), which catalyses the conversion of arachidonic acid to PGH_2 (3). The discovery of two isoforms (4), COX-1 and COX-2, helped in understanding the side effects associated with NSAIDs. COX-1 is a constitutive enzyme and is necessary for proper functioning of the kidney and stomach. In contrast, COX-2 is an inducible isoform that leads to inflammation (5, 6). Classical NSAIDs like aspirin, ibuprofen, flubriprofen and naproxen inhibit both forms of COX and cause gastric ulceration and renal failure (7–10). It is therefore expected that selective inhibition of COX-2 will provide a new generation of NSAIDs with significantly reduced side effects.

A large number of research studies aimed at finding selective COX-2 inhibitors were reported earlier (11–14). Many studies have been carried out using computer simulations to develop protocols and methods for designing new COX-2 inhibitors such as oxazoles, pyrazoles, pyrroles and imidazoles (15–19). Furthermore, selective COX-2 inhibitors are believed to play a vital role in ovulation and labor as well as in the treatment of colon cancer and Alzheimer's disease. Recently, rofecoxib has been banned from the market because of its serious side effects (20). Hence, there is a need to analyze the pharmacophore present in these compounds using the Three Dimensional Quantitative Structure Activity Relationship (3D-QSAR) methods.

Quantitative structure-activity relationship (QSAR) enables the investigators to establish reliable quantitative structure-activity and structure-property relationships to derive an *in silico* QSAR model to predict the activity of novel molecules prior to their synthesis. 3D-QSAR methodology has been successfully used to generate models for various chemotherapeutic agents.

In order to study and deduce a correlation between structure and biological activity of 5-aryl-2,2-dialkyl-4-phenyl-3(2*H*)-furanone derivatives as selective COX-2 inhibitors, we have developed 3D-QSAR CoMFA/CoMSIA models for the series of 5-aryl-2,2-dialkyl-4-phenyl-3(2*H*)-furanones (21). Together with the contour maps derived, they revealed the significance of steric, electrostatic, hydrophobic and hydrogen bond donor fields. Structural variations in the molecular fields of particular regions in the space were studied and 3D-QSAR models were generated to give an insight in the design of potent COX-2 inhibitors.

EXPERIMENTAL

Biological data

Series of 5-aryl-2,2-dialkyl-4-phenyl-3(2*H*)-furanone derivatives have been reported as selective COX-2 inhibitors (21). *In vitro* assay for COX-2 inhibition was performed using the human whole blood method. The negative logarithm of the inhibition values –log IC_{50}, *i.e.*, pIC_{50}, was used in 3D-QSAR. Tables I–III define the structure and biological activity of the training set and test set compounds. The robustness and predictive ability of the models were evaluated by selecting a wide range of biological activities with chemical classes similar to the training set.

Table I. Structures and biological activities of the training and test sets of molecules

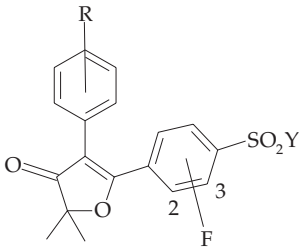

Ar – aromatic group

Compd.	Ar	R_1	R_2	Y	Biological activity[a]		
					Actual	Calculated	
						CoMFA[b]	CoMSIA
1	Phenyl	CH_3	CH_3	CH_3	7.30	7.24	7.11
2	3-Fluorophenyl	CH_3	CH_3	CH_3	7.69	7.59	7.32
3	3-Chlorophenyl	CH_3	CH_3	CH_3	8.00	6.28	6.60
4	4-Bromophenyl	CH_3	CH_3	CH_3	7.52	7.59	7.70
5[c]	3-Chloro-4-fluorophenyl	CH_3	CH_3	CH_3	6.52	7.81	7.67
6	3,5-Difluorophenyl	CH_3	CH_3	CH_3	7.30	7.51	7.34
7	3,5-Dichlorophenyl	CH_3	CH_3	CH_3	7.52	7.71	7.68
8[c]	3-(Trifluoromethyl)-phenyl	CH_3	CH_3	CH_3	7.30	7.96	7.63
9	3-*i*-Propylphenyl	CH_3	CH_3	CH_3	7.52	7.52	7.59
10	4-*i*-Propylphenyl	CH_3	CH_3	CH_3	7.52	7.47	7.43
11[c]	4-*n*-Butylphenyl	CH_3	CH_3	CH_3	8.69	7.34	7.25
12	3-Acetylphenyl	CH_3	CH_3	CH_3	7.30	7.44	7.15
13	4-Acetylphenyl	CH_3	CH_3	CH_3	6.52	6.68	6.68
14	3-Methoxyphenyl	CH_3	CH_3	CH_3	7.00	7.03	7.03
15	Phenyl	CH_3	C_2H_5	CH_3	6.69	6.74	6.84
16	2-Fluorophenyl	CH_3	C_2H_5	CH_3	6.52	6.72	6.79
17	3-Chlorophenyl	CH_3	C_2H_5	CH_3	7.52	7.31	7.32
18	3,5-Dichlorophenyl	CH_3	C_2H_5	CH_3	7.52	7.34	7.40
19	3-(Trifluoromethyl)-phenyl	CH_3	C_2H_5	CH_3	7.30	7.33	7.40
20[c]	3-Methoxyphenyl	CH_3	C_2H_5	CH_3	6.52	7.68	6.79
21	Phenyl	C_2H_5	C_2H_5	CH_3	6.69	6.82	6.92
22	4-(Trifluoromethyl)-phenyl	C_2H_5	C_2H_5	CH_3	7.52	7.55	7.42
23[c]	3-Methylphenyl	C_2H_5	C_2H_5	CH_3	6.30	7.09	7.19
24	4-Methylphenyl	C_2H_5	C_2H_5	CH_3	7.52	7.33	7.17
25	Phenyl	CH_3	CH_3	NH_2	8.09	7.96	8.13
26	3-Fluorophenyl	CH_3	CH_3	NH_2	8.52	8.53	8.35
27	3,4-Difluorophenyl	CH_3	CH_3	NH_2	8.15	7.05	7.25
28[c]	3-(Trifluoromethyl)-phenyl	CH_3	CH_3	NH_2	7.95	8.89	8.67
29	4-Acetylphenyl	CH_3	CH_3	NH_2	7.88	7.61	7.70

[a] Biological activity (μmol L^{-1}) expressed as –log IC_{50} against human COX–2 enzyme.
[b] Calculated activity from alignment IV.
[c] Test set molecules.

Table II. Training and test sets of molecules

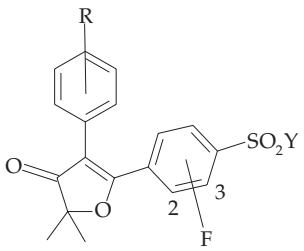

Compd.	Fluoride position	R	Y	Biological activity[a]		
				Actual	Calculated	
					CoMFA[b]	CoMSIA
30[c]	2	H	CH_3	7.52	7.21	7.24
31[c]		3-F	CH_3	7.52	7.18	7.32
32		3-Cl	CH_3	7.69	7.74	7.68
33		3-F, 5-F	CH_3	7.52	7.58	7.42
34[c]	3	H	CH_3	7.52	6.64	7.11
35		3-F	CH_3	7.52	7.09	7.32
36		3-Cl	CH_3	7.36	7.20	7.59
37[c]		3-F, 5-F	CH_3	7.52	6.95	7.33
38[c]	2	H	NH_2	7.52	7.96	8.40
39		3-F	NH_2	8.52	8.55	8.62
40		3-F, 5-F	NH_2	8.52	8.45	8.64
41	3	H	NH_2	7.52	7.45	7.45
42		3-F	NH_2	7.52	7.89	7.66
43[c]		3-F, 5-F	NH_2	7.69	7.79	7.67

[a] Biological activity (μmol L^{-1}) expressed as –log IC_{50} against human COX–2 enzyme.
[b] Calculated activity from alignment IV.
[c] Test set molecules.

Molecular modeling

All molecular modeling and 3D-QSAR studies were performed using the molecular modeling package SYBYL 6.9 (22) with standard Tripos force field (23) at the Silicon Graphics Fuel workstation. The X-ray crystallographic data for this ligand-COX-2 complex are not deposited in the protein data bank; hence all the molecules were constructed using the standard geometry and bond lengths with SYBYL. The initial optimization was carried out using the standard TRIPOS force field employing the Gasteiger Marsili charges; the constraints were removed and repeated minimization was performed using the steepest descent and conjugated gradient method until the RMSD (root mean square deviation)

Table III. Structures and biological activities of the training and test sets of molecules

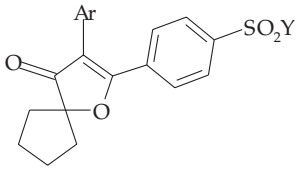

44–47

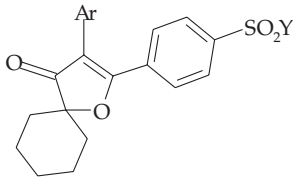

48–49

Ar–aromatic group

Compd.	Ar	Biological activity[a]		
		Actual	Calculated	
			CoMFA[b]	CoMSIA
44[c]	Phenyl	7.52	7.08	7.12
45	3-Fluorophenyl	6.47	7.93	7.80
46	3-Methylphenyl	7.52	7.36	7.39
47	4-*i*-Propylphenyl	7.30	7.40	7.44
48	Phenyl	6.30	6.16	6.15
49	3-Methylphenyl	6.30	6.46	6.46

[a] Biological activity (μmol L^{-1}) expressed as –log IC_{50} against human COX–2 enzyme.
[b] Calculated activity from alignment IV.
[c] Test set molecules.

value of 0.001 kcal mol^{-1} was achieved. Using MULTISEARCH option in SYBYL 6.9, various conformers were obtained out of which the lowest energy conformers were selected for superimposition. Further geometry optimization was performed using MOPAC with AM1 Hamiltonian (24).

Alignment rules

Molecular conformation and orientation is one of the most sensitive input areas in 3D-QSAR studies. In the present study, superimposition of the molecules was carried out by different approaches using compound **26** (Table I) as template structure.

Alignment I. – Each analog was aligned to the template by rotation and translation so as to minimize the RMSD between atoms in the template and the corresponding atoms in the analog using the DATABASE ALIGN option in SYBYL.

Alignment II. – In this alignment, atoms of the molecules were used for RMS (root mean square) fitting corresponding to the atoms in the template.

Alignment III. – Here, centroids rather than the exact superimposition of atoms of the rings were used for RMS fitting to the template.

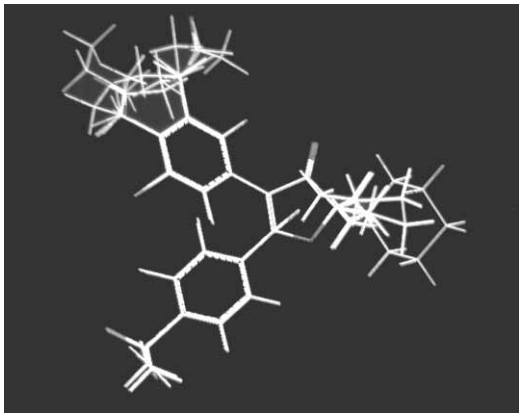

Fig. 1. Superimposition of 49 molecules obtained by alignment IV.

Alignment IV. – Here, both atoms and centroids were selected for superimposition on the template. Fig. 1 shows the superimposition of 49 molecules obtained by alignment IV. The atoms and centroids used for alignments are defined in Fig. 2. These alignments were subsequently used in CoMFA/CoMSIA probe interaction energy calculations.

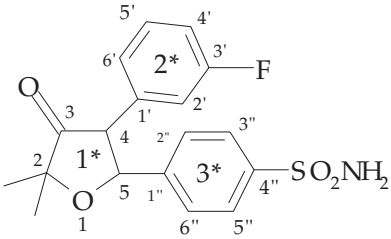

Template molecule (**26**)

Alignment	Atoms/centroids
I	Database alignment
II	2, 4, 1′, 5, 1″
III	1*, 2*, 3*
IV	1*, 4, 1′, 5, 1″

Fig. 2. Alignment rules.

CoMFA and CoMSIA studies

The steric and electrostatic field energies were calculated using sp^3 carbon as probe atom. The energies were truncated to ± 30 kcal mol^{-1}. The CoMFA fields generated automatically were scaled by the CoMFA-STD method in SYBYL.

Similarity indices (descriptors) were derived with the same lattice box as used in CoMFA calculations. Five CoMSIA similarity index fields available within SYBYL [steric, electrostatic, hydrophobic (lipophilic), hydrogen bond donor, hydrogen bond acceptor] were evaluated using the probe atom. Gaussian-type distance dependence was between the grid point and each atom of the molecule. The default value of 0.3 was used as attenuation factor.

Partial least square (PLS) analysis

The CoMFA/CoMSIA descriptors served as independent variables and pIC_{50} values as a dependent variable in PLS regression analysis (25) in deducing the 3D-QSAR models. Normally, cross-validation is used to check the predictivity of the derived model. Results of the analyses correspond to a regression equation with thousands of coefficients. The performance of models was calculated using the leave one out (LOO) cross--validation method. The optimum number of components (Nc) used to derive the non cross-validated model was defined as the number of components leading to the highest R^2 cross-validated and lowest standard error of prediction (SEP). To obtain the statistical confidence limit in analyses, PLS analysis using 100 bootstrap groups within the optimum number of components was performed.

RESULTS AND DISCUSSION

CoMFA and CoMSIA techniques were used to derive 3D-QSAR models for 5-aryl--2,2-dialkyl-4-phenyl-3(2*H*)-furanones as selective COX-2 inhibitors. The negative logarithm of the *in vitro* inhibitory activity pIC_{50} was used as a dependent variable.

The lower energy conformers obtained from the MULTISEARCH option in SYBYL were used in the study. All the molecules were aligned employing atom/shape based RMS fitting and RMSD based database fitting techniques. Various 3D-QSAR models were generated and the best one was selected based on the statistically significant parameters obtained.

Preliminary studies performed using 39 molecules in the training set reveal the significance of CoMFA parameters for the final results. PLS analysis was performed using varying column filtering values. Finally, column filtering was set to 0.0 kcal mol^{-1} and used for further calculations in PLS analysis.

Analysis A shows CoMFA results (Table IV) obtained from four different alignments using 39 molecules in the training set. Database alignment I showed cross-validated R^2 = 0.416 with four components, non cross-validated R^2 = 0.809, *F* value 18.850, bootstrapped R^2 = 0.909; the steric and electrostatic contributions were 70.1 and 29.9%, respectively.

The CoMFA model generated from atom based RMS alignment II (Table IV) showed cross-validated R^2 = 0.389 with four components, non cross-validated R^2 = 0.846, *F* value 43.806, bootstrapped R^2 = 0.899 with 60.2 steric and 39.8% electrostatic contributions.

The shape based alignment III (Table IV) yielded cross-validated R^2 = 0.322 with five components, non cross-validated R^2 = 0.759, *F* value 35.670 and bootstrapped R^2 = 0.806. The steric and electrostatic contributions were 68.3 and 31.7%, respectively.

Table IV. Summary of CoMFA results (analysis A)

Alignment	I[a]	II[b]	III[c]	IV[d]
R^2_{cv}[e]	0.416	0.389	0.322	0.429
Nc[f]	4	4	5	5
SEP[g]	0.493	0.543	0.540	0.470
R^2_{ncv}[h]	0.809	0.846	0.759	0.822
SEE[i]	0.284	0.273	0.292	0.262
F value	18.850	43.806	35.670	28.664
P $R^2 = 0$[j]	0.0	0.0	0.0	0.0
Contrib. steric	70.1	60.2	68.3	64.3
Contrib. electr.	29.9	39.8	31.7	35.7
R^2_{bs}[k]	0.909	0.899	0.806	0.890
SD[l]	0.034	0.044	0.060	0.039

[a] Alignment by RMSD database.
[b] Alignment by atom-based RMS fit.
[c] Alignment by shape-based RMS fit.
[d] Alignment by atom and shape-based RMS fit.
[e] Cross-validated correlation coefficient.
[f] Number of components.
[g] Standard error of prediction.
[h] Non cross-validated square of correlation coefficient.
[i] Standard error of estimate.
[j] P $R^2 = 0$, probability that correlation coefficient *R* equals zero.
[k] From 100 bootstrapping runs.
[l] Standard deviation.

Alignment IV (atom and shape based) yielded a cross-validated $R^2 = 0.429$ with five components, non cross-validated $R^2 = 0.822$, *F* value 28.664 and bootstrapped $R^2 = 0.890$. The steric and electrostatic contributions were 64.3 and 35.7%, respectively.

Since the CoMFA technique is alignment sensitive, differences in statistical values are observed with different alignments (Table IV). All the CoMFA models obtained from analysis A demonstrated moderate internal and external predictivity. Thus, in order to increase the predictive power of derived models, further experiments were performed. Based on the results of the QSAR studies, three molecules (**3, 27** and **45**) of the training set with high residual values were omitted from the PLS analysis.

Analysis B (Table V) shows the CoMFA results obtained from four different alignments using a training set involving 36 molecules; the model derived showed a better confidence level in statistical significance.

RMSD based database alignment I showed improved cross-validated R^2 value of 0.416–0.502 with five components, non cross-validated $R^2 = 0.809$–0.922, *F* value 18.850–34.292 and bootstrapped R^2 between 0.909 and 0.969. The steric and electrostatic contributions were found to be 58.2 and 41.8%, respectively. The same trend was observed in the remaining alignments (Table V), except that for atom-based alignment II the *F* value slightly decreased from 43.806 to 40.416. This model displayed an improved cross-validated R^2 of 0.389 to 0.559 with five components, non cross-validated R^2 from 0.846 to

Table V. Summary of CoMFA results (analysis B)

Alignment	I[a]	II[b]	III[c]	IV[d]
R^2_{cv}[e]	0.502	0.559	0.652	0.664
Nc[f]	5	5	6	6
SEP[g]	0.430	0.405	0.361	0.360
R^2_{ncv}[h]	0.922	0.893	0.914	0.916
SEE[i]	0.183	0.203	0.179	0.180
F value	34.292	40.416	48.127	47.341
P $R^2 = 0$[j]	0.0	0.0	0.0	0.0
Contrib. steric	58.2	59.4	59.9	58.1
Contrib. electr.	41.8	40.6	40.1	41.9
R^2_{bs}[k]	0.969	0.913	0.946	0.947
SD[l]	0.017	0.034	0.025	0.029

[a] Alignment by RMSD database.
[b] Alignment by atom-based RMS fit.
[c] Alignment by shape-based RMS fit.
[d] Alignment by atom and shape-based RMS fit.
[e] Cross – validated correlation coefficient.
[f] Number of components.
[g] Standard error of prediction.
[h] Non cross-validated square of correlation coefficient.
[i] Standard error of estimate.
[j] P $R^2 = 0$, probability that correlation coefficient *R* equals zero.
[k] From 100 bootstrapping runs.
[l] Standard deviation.

0.893 and bootstrapped R^2 from 0.899 to 0.913 with 59.4 and 40.6% steric and electrostatic contributions, respectively.

The shape based alignment III (Table V) yielded cross-validated $R^2 = 0.652$ with six components, non cross-validated R^2 of 0.914, R^2 value 48.127 and bootstrapped R^2 of 0.946. The steric and electrostatic contributions were 59.9 and 40.1%, respectively.

Alignment IV (Table VI) yielded the highest cross-validated R^2 of 0.664 with six components, non cross-validated R^2 of 0.916, *F* value 47.347 and bootstrapped R^2 of 0.947. The steric and electrostatic contributions were found to be 58.1 and 41.9%, respectively.

Thus, all the CoMFA models derived from analysis B showed higher contributions of steric parameters to the activity of these compounds similar to that of analysis A. Based on the predictive ability of the four CoMFA models from analysis B, alignment IV was selected for further analysis and all the CoMFA contours were generated using this model. The graphs of actual *vs.* fitted and predicted activities for the training and test sets of molecules are depicted in Figs. 3a and 3b, respectively. The field values generated at each grid point were calculated as the scalar product of the associated QSAR coefficient and the standard deviation of all values in the corresponding column of the data table (STDDEV*COEFF), plotted as the percentage contributions to QSAR equation. The CoMFA steric and electrostatic contour maps developed using the alignment IV analyses are shown in Figs. 4a and 4b, respectively.

Table VI. Summary of CoMSIA results

	S[a]+E[b]+H[c]	S+E+D[d]	S+E+A[e]	S+E+D+A	H+D+A	S+E+D+H	S+E+H+A	S+D+A	All[n]
R^2_{cv}[f]	0.635	0.722	0.507	0.705	0.648	0.777	0.641	0.710	0.739
Nc[g]	3	4	7	3	4	4	6	5	5
SEP[h]	0.355	0.316	0.445	0.319	0.355	0.282	0.372	0.328	0.311
R^2_{ncv}[i]	0.844	0.852	0.890	0.831	0.901	0.905	0.902	0.819	0.918
SEE[j]	0.232	0.230	0.210	0.242	0.188	0.185	0.194	0.259	0.175
F value	52.48	40.280	28.766	47.548	63.65	66.322	40.092	24.47	60.145
P $R^2 = 0$[k]	0.0	0.0	0.0	0.0	0.0	0.0	0.0	0.0	0.0
R^2_{bs}[l]	0.880	0.896	0.944	0.848	0.925	0.933	0.946	0.882	0.945
SD[m]	0.044	0.039	0.031	0.055	0.030	0.028	0.036	0.055	0.026

[a] Steric.
[b] Electrostatic.
[c] Hydrophobic.
[d] Hydrogen bond donor.
[e] Hydrogen bond acceptor.
[f] Cross-validated correlation coefficient.
[g] Number of components.
[h] Standard error of prediction.
[i] Non cross-validated square of correlation coefficient.
[j] Standard error of estimate.
[k] P $R^2 = 0$, probability that correlation coefficient *R* equals zero.
[l] From 100 bootstrapped runs.
[m] Standard deviation.
[n] All = S+E+D+A+H.

The CoMFA steric map (Fig. 4a) encompasses sterically unfavorable contours (80% contribution) corresponding to regions in space where steric bulk envisages the decrease in activity and the polyhedron bordering the furanone ring suggests that bulkier substituents are not favorable in that region. Conversely, the sterically favorable regions (20% contribution) observed on the upper side of the 4-phenyl ring in the vicinity of 5′-F of compound **26** reveal that an increase in activity is anticipated due to the increased steric bulk. Steric substituents at 3′ and 4′ positions favor the activity (compound **11**). In this compound, the structural flexibility of the *n*-butyl moiety seems to allow it to maneuver into the ideal space for COX-2 activity and selectivity. However, the sterically unfavorable contours surrounding 2-position of the furanone nucleus suggested that high steric bulk reduces the activity (compounds **47**–**49**). Compounds containing the spirocyclopentyl moiety (compounds **44**–**47**) at 2-position in the furanone nucleus showed better activity compared to compounds **21**–**24**. This may be due to the spirocyclopentyl moiety occupying a smaller space compared to the diethyl moiety in compounds **21**–**24**. According to the reported structure of COX-2, there should be a cavity of limited size available to the 2,2-dialkyl moiety of 3(2*H*)-furanone COX-2 inhibitors. Spirocyclohexyl moiety containing compounds (**48** and **49**) show even poorer activity, which supports the rationale for »the cavity of limited size near the entrance of COX-2 active site«.

The CoMFA electrostatic map (Fig. 4b), displays contours in the vicinity of 4′-H and 5′-H where the partial negative charge is associated with increased activity (80% contribution). Contours observed in the vicinity of sulfonamide group of 5-phenyl ring (20%

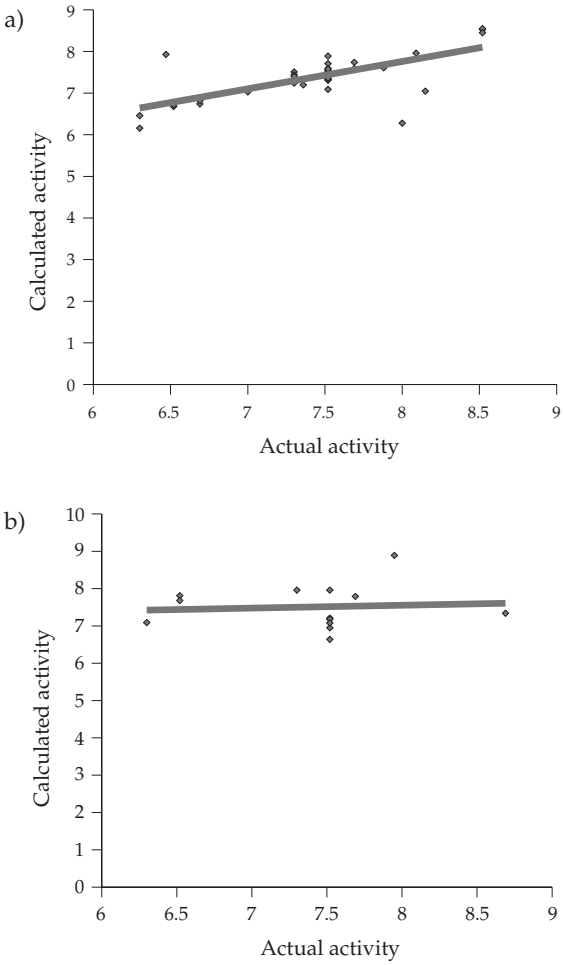

Fig. 3. Graph of actual *vs.* calculated activities from alignment IV (analysis B) of: a) training set molecules, b) test set molecules.

contribution) of compound **26** indicate areas where the electropositive properties of molecules indicate an increase in activity. The electronegative group favoring contours (Fig. 4b) in the vicinity of 3′-H and 4′-H suggest that increased activity is anticipated by electronegative substituents at positions 3′ and 4′ (compounds **26** and **40**), whereas the electropositive favoring contour indicates low electron density substituents at 4′′-position favoring activity.

In addition to steric and electrostatic fields, CoMSIA also defines the lipophilicity, hydrogen bond donor and acceptor fields that are not generally accessible with standard CoMFA. The atom and shape based alignment IV used in CoMFA studies served as an alignment for CoMSIA and the results of the study are summarized in Table VI.

The CoMSIA model with the combination of all fields yielded a cross-validated R^2 = 0.739 with five components, non cross-validated R^2 = 0.918, F value 60.145 and bootstrap-

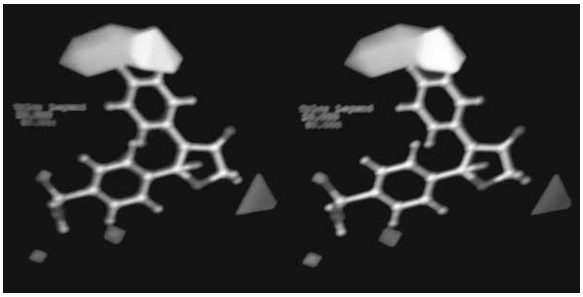

Fig. 4a. Stereoview of CoMFA steric STDDEV*COEFF contour plots from alignment IV (analysis B). Sterically favored areas (contribution level 80%) are represented by contours at the top of the molecule as shown above. Sterically disfavored areas (contribution level 20%) are represented by polyhedra in the vicinity the of five-membered ring. Active compound **26** in ball and stick is shown.

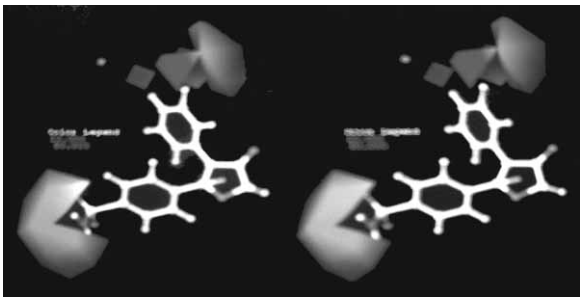

Fig. 4b. Stereoview of CoMFA electrostatic STDDEV*COEFF contour plots from alignment IV (analysis B). Positively charged favored areas (contribution level 80%) are represented by polyhedra (left corner). Negatively charged favored areas (contribution level 20%) are represented by polyhedra at the top. Active compound **26** in ball and stick is shown.

ped R^2 = 0.945. The contributions of steric, electrostatic, hydrophobic, hydrogen bond donor and acceptor fields of this model were 8.2, 8.1, 25.1 and 27.7%, respectively.

The CoMSIA model with the combination of steric, electrostatic, hydrophobic and hydrogen bond donor fields yielded the highest cross-validated R^2 = 0.777 with four components, non cross-validated R^2 = 0.905, F value 66.322 and bootstrapped R^2 of 0.933. The steric, electrostatic, hydrophobic and hydrogen bond donor field contributions were 12.6, 11.0, 34.4 and 41.9%, respectively.

Combinations of steric, electrostatic and hydrogen bond donor fields yielded a CoMSIA model with a cross-validated R^2 = 0.722 with four components, non cross-validated R^2= 0.852, F value 40.280 and bootstrapped R^2 = 0.896. The steric, electrostatic and hydrogen bond donor contributions were 31.3, 21.9 and 46.9%, respectively.

The models generated by various combinations of CoMSIA fields (Table VI) show statistically significant, moderate to high, internal and external predictions, in which the hydrogen bond donor fields were observed to be predominant over the hydrophobic and hydrogen bond acceptor fields. The graphs of actual *vs.* fitted and predicted activi-

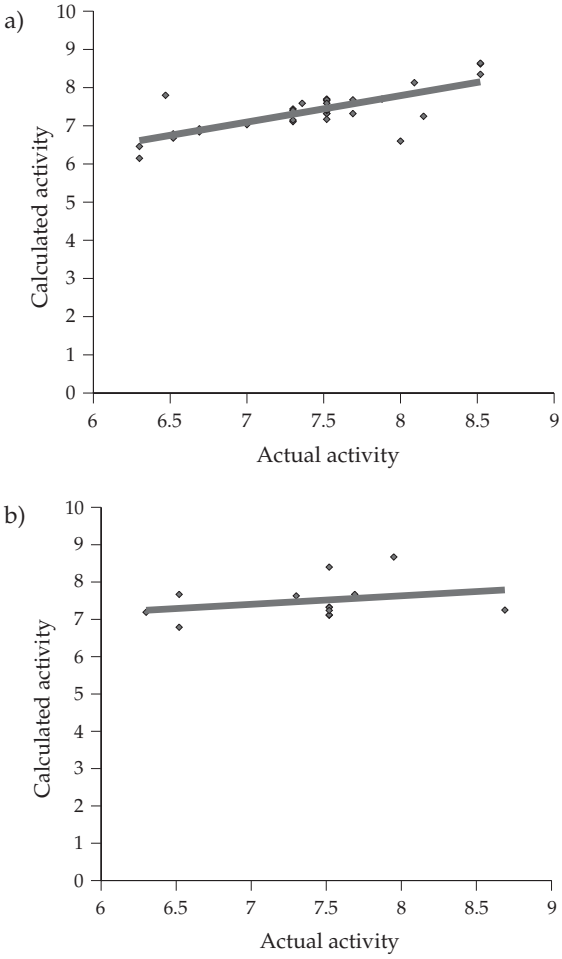

Fig. 5a. Graph of actual *vs.* predicted activities from CoMSIA analysis with steric, electrostatic, hydrophobic and hydrogen bond donor fields for: a) training set molecules, b) test set molecules.

ties for the training and test set molecules from all CoMSIA fields are shown in Figs. 5a and 5b, respectively. The CoMSIA steric and electrostatic contours (not shown) were positioned similarly to those of the CoMFA model. The hydrogen bond donor contour maps of CoMSIA (STDDEV*COEFF) are displayed in Fig. 6a. The contour region (80% contribution) near 3′′-H of the 5-phenyl ring and also in the vicinity of 3′-F and 4′-H of the 4-phenyl ring indicate the disfavored regions for hydrogen bond donor substituents. However, the contour region (20% contribution) in the lower region of the 5-phenyl ring, in the vicinity of 5′′-H of compound **26**, indicates favored regions for hydrogen bond donor substituents.

The hydrophobic contour maps of CoMSIA (STDDEV*COEFF) are displayed in Fig. 6b. The contours covering the five membered furanone ring indicate disfavored regions, while the contours in the vicinity of 3′-F, 4′-H and 5′-H of the 4-phenyl ring of compound **26** indicate favored regions.

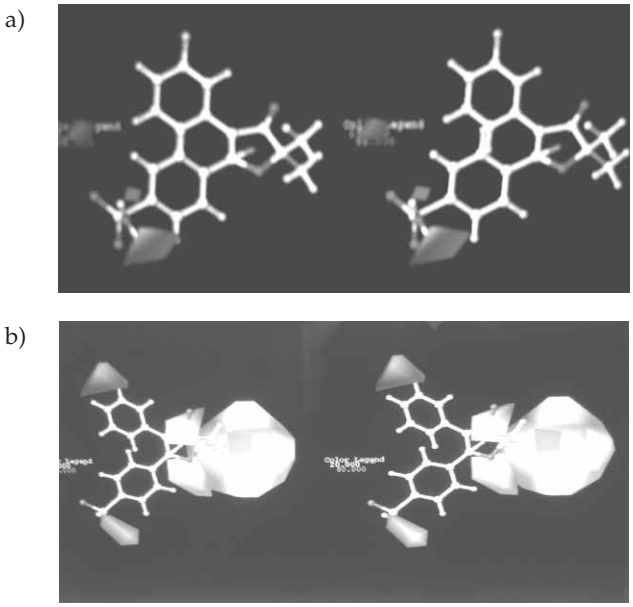

Fig. 6. Stereoview of CoMSIA of: a) hydrogen bond donor fields, b) hydrophobic fields.

The CoMSIA QSAR studies give an additional structural insight into the study of the probable binding sites of the ligand-receptor. The hydrogen bond donor favorable contour in the vicinity of the amino group of sulfonamide moiety indicates the significance of the proton in the hydrogen bond formation of the receptor surface. Disfavorable contours in the upper region of the 4-phenyl ring indicate that hydrogen bond donor substituents on this ring decrease activity (compounds **13** and **23**). The hydrophobic field favoring contours (Fig. 6b) in the upper region of the 4-phenyl ring highlight the significance of hydrophobic groups on 3′-H, 4′-H and 5′-H of the 4-phenyl ring in the biological activity, whereas the disfavoring contours surrounding the furanone ring indicate that hydrophobic substitutions on this five-membered ring decrease activity (compounds 45–49).

The present results of 3D-QSAR studies are in agreement with the *in vitro* COX-2 inhibitory activity as reported by Shin *et al.* (21).

CONCLUSIONS

A receptor independent 3D-QSAR has been established for 5-aryl-2,2-dialkyl-4-phenyl-3(2*H*)-furanones as selective COX-2 inhibitors employing the most widely used techniques CoMFA and CoMSIA. The present studies highlight the importance of ligand orientation and selection of the training set molecules in the development of statistically significant QSAR models. CoMSIA models provided better statistical models than CoMFA,

which points to the significance of hydrogen bond donor and hydrophobic fields in the selectivity and activity of these ligands in addition to steric and electrostatic fields. The statistical significance and robustness of generated 3D-QSAR models were confirmed using an external set of molecules. The structural requirements identified in the present study can be utilized strategically in the design of novel, potent and selective cyclooxygenase-2 inhibitors as anti-inflammatory agents.

Supporting information. – SMILES format for molecules used in the QSAR analysis
C. No 1. O1[CH](=[CH](C(=O)C1(C)C)c2ccccc2)c3ccc(cc3)S(=O)(=O)C
C. No 2. O1[CH](=[CH](C(=O)C1(C)C)c2cc(ccc2)F)c3ccc(cc3)S(=O)(=O)C
C. No 3. O1[CH](=[CH](C(=O)C1(C)C)c2cc(ccc2)Cl)c3ccc(cc3)S(=O)(=O)C
C. No 4. O1[CH](=[CH](C(=O)C1(C)C)c2ccc(cc2)Br)c3ccc(cc3)S(=O)(=O)C
C. No 5. O1[CH](=[CH](C(=O)C1(C)C)c2cc(c(cc2)F)Cl)c3ccc(cc3)S(=O)(=O)C
C. No 6. O1[CH](=[CH](C(=O)C1(C)C)c2cc(cc(c2)F)F)c3ccc(cc3)S(=O)(=O)C
C. No 7. O1[CH](=[CH](C(=O)C1(C)C)c2cc(cc(c2)Cl)Cl)c3ccc(cc3)S(=O)(=O)C
C. No 8. O1[CH](=[CH](C(=O)C1(C)C)c2cc(ccc2)C(F)(F)F)c3ccc(cc3)S(=O)(=O)C
C. No 9. O1[CH](=[CH](C(=O)C1(C)C)c2cc(ccc2)C(C)C)c3ccc(cc3)S(=O)(=O)C
C. No 10.O1[CH](=[CH](C(=O)C1(C)C)c2ccc(cc2)C(C)C)c3ccc(cc3)S(=O)(=O)C
C. No 11. O1[CH](=[CH](C(=O)C1(C)C)c2ccc(cc2)CCCC)c3ccc(cc3)S(=O)(=O)C
C. No 12. O1[CH](=[CH](C(=O)C1(C)C)c2cc(ccc2)C(=O)C)c3ccc(cc3)S(=O)(=O)C
C. No 13. O1[CH](=[CH](C(=O)C1(C)C)c2ccc(cc2)C(=O)C)c3ccc(cc3)S(=O)(=O)C
C. No 14. O1[CH](=[CH](C(=O)C1(C)C)c2cc(ccc2)OC)c3ccc(cc3)S(=O)(=O)C
C. No 15. O1[CH](=[CH](C(=O)C1(CC)C)c2ccccc2)c3ccc(cc3)S(=O)(=O)C
C. No 16. O1[CH](=[CH](C(=O)C1(CC)C)c2c(cccc2)F)c3ccc(cc3)S(=O)(=O)C
C. No 17. O1[CH](=[CH](C(=O)C1(CC)C)c2cc(ccc2)Cl)c3ccc(cc3)S(=O)(=O)C
C. No 18. O1[CH](=[CH](C(=O)C1(CC)C)c2cc(cc(c2)Cl)Cl)c3ccc(cc3)S(=O)(=O)C
C. No 19. O1[CH](=[CH](C(=O)C1(CC)C)c2cc(ccc2)C(F)(F)F)c3ccc(cc3)S(=O)(=O)C
C. No 20. O1[CH](=[CH](C(=O)C1(CC)C)c2cc(ccc2)[OH3])c3ccc(cc3)S(=O)(=O)C
C. No 21. O1[CH](=[CH](C(=O)C1(CC)CC)c2ccccc2)c3ccc(cc3)S(=O)(=O)C
C. No 22. O1[CH](=[CH](C(=O)C1(CC)CC)c2ccc(cc2)C(F)(F)F)c3ccc(cc3)S(=O)(=O)C
C. No 23. O1[CH](=[CH](C(=O)C1(CC)CC)c2cc(ccc2)C)c3ccc(cc3)S(=O)(=O)C
C. No 24. O1[CH](=[CH](C(=O)C1(CC)CC)c2ccc(cc2)C)c3ccc(cc3)S(=O)(=O)C
C. No 25. O1[CH](=[CH](C(=O)C1(C)C)c2ccccc2)c3ccc(cc3)S(=O)(=O)N
C. No 26. O1[CH](=[CH](C(=O)C1(C)C)c2cc(ccc2)F)c3ccc(cc3)S(=O)(=O)N
C. No 27. O1[CH](=[CH](C(=O)C1(C)C)c2cc(c(cc2)F)F)c3ccc(cc3)S(=O)(=O)N
C. No 28. O1[CH](=[CH](C(=O)C1(C)C)c2cc(ccc2)C(F)(F)F)c3ccc(cc3)S(=O)(=O)N
C. No 29. O1[CH](=[CH](C(=O)C1(C)C)c2ccc(cc2)C(=O)C)c3ccc(cc3)S(=O)(=O)N
C. No 30. O1[CH](=[CH](C(=O)C1)c2ccccc2)c3ccc(cc3F)S(=O)(=O)C
C. No 31. O1[CH](=[CH](C(=O)C1)c2cc(ccc2)F)c3ccc(cc3F)S(=O)(=O)C
C. No 32. O1[CH](=[CH](C(=O)C1)c2cc(ccc2)Cl)c3ccc(cc3F)S(=O)(=O)C
C. No 33. O1[CH](=[CH](C(=O)C1)c2cc(cc(c2)F)F)c3ccc(cc3F)S(=O)(=O)C
C. No 34. O1[CH](=[CH](C(=O)C1)c2ccccc2)c3ccc(c(c3)F)S(=O)(=O)C
C. No 35. O1[CH](=[CH](C(=O)C1)c2cc(ccc2)F)c3ccc(c(c3)F)S(=O)(=O)C
C. No 36. O1[CH](=[CH](C(=O)C1)c2cc(ccc2)Cl)c3ccc(c(c3)F)S(=O)(=O)C
C. No 37. O1[CH](=[CH](C(=O)C1)c2cc(cc(c2)F)F)c3ccc(c(c3)F)S(=O)(=O)C
C. No 38. O1[CH](=[CH](C(=O)C1)c2ccccc2)c3ccc(cc3F)S(=O)(=O)N
C. No 39. O1[CH](=[CH](C(=O)C1)c2cc(ccc2)F)c3ccc(cc3F)S(=O)(=O)N
C. No 40. O1[CH](=[CH](C(=O)C1)c2cc(cc(c2)F)F)c3ccc(cc3F)S(=O)(=O)N
C. No 41. O1[CH](=[CH](C(=O)C1)c2ccccc2)c3ccc(c(c3)F)S(=O)(=O)N
C. No 42. O1[CH](=[CH](C(=O)C1)c2cc(ccc2)F)c3ccc(c(c3)F)S(=O)(=O)N
C. No 43. O1[CH](=[CH](C(=O)C1)c2cc(cc(c2)F)F)c3ccc(c(c3)F)S(=O)(=O)N

C. No 44. O1[CH](=[CH](C(=O)C21CCCC2)c3ccccc3)c4ccc(cc4)S(=O)(=O)C
C. No 45. O1[CH](=[CH](C(=O)C21CCCC2)c3cc(ccc3)F)c4ccc(cc4)S(=O)(=O)C
C. No 46. O1[CH](=[CH](C(=O)C21CCCC2)c3cc(ccc3)C)c4ccc(cc4)S(=O)(=O)C
C. No 47. O1[CH](=[CH](C(=O)C21CCCC2)c3ccc(cc3)C(C)C)c4ccc(cc4)S(=O)(=O)C
C. No 48. O1[CH](=[CH](C(=O)C21CCCCC2)c3ccccc3)c4ccc(cc4)S(=O)(=O)C
C. No 49. O1[CH](=[CH](C(=O)C21CCCCC2)c3cc(ccc3)[C])c4ccc(cc4)S(=O)(=O)C

REFERENCES

1. P. Mantri and D. Witiak, Inhibitors of COX and 5-Lipoxygenase, *Curr. Med. Chem.* **1** (1994) 328–355.
2. J. R. Vane and R. Botting, Mechanism of action of anti-inflammatory drugs, *Scand. T. Rheumatol. Suppl.* **102** (1996) 9–21.
3. W. L. Smith, P. Borgeat and F. A. Fitzpatrik, *The Eicosanoids: COX, Lipoxygenase and Epoxygenase Pathways*, in *Biochemistry of Lipids, Lipoproteins and Membranes* (Ed. D. E. Vance), Elsevier, New York 1991, pp. 297–325.
4. W. Xie, J. Chipman, D. L. Robertson, R. L. Erikson and D. L. Simmons, Expression of mitogen response gene encoding prostaglandin synthase regulated by mRNA splicing, *Proc. Natl. Acad. Sci. U.S.A.* **88** (1991) 2692–2696.
5. J. R. Vane and R. M. Botting, Antiinflammatory drugs and their mechanism of action, *Inflammation Res.* **47** (1998) S78–S87.
6. M. Katori and M. Majima, Possible background mechanisms of the effectiveness of COX-2 inhibitors in treatment of rheumatoid arthritis, *Inflammation Res.* **47** (1998) S107–S111.
7. D. L. Dewitt, COX-2 Inhibitors: The super new aspirins, *Mol. Pharmacol.* **4** (1999) 625–631.
8. L. J. Marnett and A. S. Kalgutkar, Design of selective inhibitors of COX-2 as non-ulcerogenic antiinflammatory agents, *Curr. Opin. Chem. Biol.* 2 (*1998*) 482–490.
9. C. J. Hawkey, COX-2 Inhibitors, *Lancet* **353** (1999) 307–314.
10. J. R. Vane and R. Botting, *Clinical Significance and Potential of Selective COX-2 Inhibition*, William Harvey Press, London 1998.
11. R. G. Kurumbail, A. M. Stevens, J. K. Gierse, J. J. McDonald, R. A. Slegeman, J. Y. Pak, D. I. Gildehaus, J. M. Miyashiro, T. D. Penning, K. Siebert, P. C. Isakson and W. C. Stallings, Structural basis of selective inhibition of COX-2 by anti-inflammatory agents, *Nature* **384** (1996) 644–648.
12. Y. Leblanc, W. C. Black, C. C. Chan, S. Charleson, D. Delorme, D. Denis, J. Y. Gautheir, E. L. Grimm, R. Gardon, D. Guay, P. Hamel, S. Kargman, C. K. Lau, J. I. Mancini, M. Ouellet, D. Percival, P. Roy, K. Skorey, P. Tagari, E. Wong, L. Xu and P. Prasit, Synthesis and biological evaluation of both enantiomers of L-761000 as inhibitors of cyclooxygenase-1 and 2, *Bioorg. Med. Chem. Lett.* **6** (1996) 731–736.
13. K. M. Woods, R. W. McCroskey and M. R. Michaelides, Heterocyclic compounds as COX-2 inhibitors, World Patent WO989330, 4 March 1997**.**
14. T. Klein, R. M. Nusing, J. Pfeilschifetr and V. Ulrich, Selective inhibition of COX-2, *Biochem. Pharmacol.* **48** (1994) 1605–1610.
15. P. Chavatte, S. Yous, C. Maro, N. Baurin and D. Lesieur, Three dimensional quantitative structure activity relationships of cyclooxygenase-2: A comparative molecular field analysis, *J. Med. Chem.* **44** (2001) 3223–3230.
16. J. R. Desiraju, B. Gopalkrishnan, R. K. R. Jetti, A. Nagaraju, D. Ravindra, J. R. P. Sarma and M. E. Sobhia, Computer aided drug design of selective COX-2 inhibitors: CoMFA, CoMSIA and docking studies of some 1,2 diarylimidazole derivatives, *J. Med. Chem.* **45** (2002) 4847–4855.

17. H. Liu, X. Q. Huang, S. J. Shen, X. M. Luo, M. H. Li, B. Xiong, G. Chen, J. K. Shen, Y. M. Yang and K. X. Chen, Inhibitory mode of 1,5 diarylpyrazole derivatives against cyclooxygenase-2 and cyclooxygenase-1, *J. Med. Chem.* **45** (2002) 4816–4827.
18. R. Solvia, C. Almansa, S. G. Kalko, S. J. Luque and M. Brozco, Theoretical studies on the inhibition mechanisms of COX-2: Is there a unique recognition site? *J. Med. Chem.* **46** (2003) 1372–1377.
19. R. Garg, A. Kurup, S. B. Mekapati and C. Hansch, Cyclooxygenase inhibition: A comparative QSAR study, *Chem. Rev.* **102** (2003) 703–732.
20. E. J. Topol, Failing the public health – Rofecoxib, Merck and the FDA, *New Engl. J. Med.* **351** (2004) 1707–1709.
21. S. S. Shin, Y. Byun, K. M. Lim, J. K. Choi, K. Lee, J. H. Mon, J. K. Kim, Y. S. Jeong, J. Y. Kim, H. J. Koh, Y. H. Park, M. S. Noh and S. Chung, *In vitro* SAR and *in vivo* studies for a novel class of COX-2 inhibitors: 5-aryl-2,2 dialkyl-4-phenyl-3(2*H*) furanone derivatives, *J. Med. Chem.* **47** (2004) 792–804.
22. SYBYL 6.9, Tripos Associates, St. Louis, MO, USA.
23. M. Clark, R. R. Crammer and O. N. Van, The tripos force field, *J. Comput. Chem.* **10** (1989) 982–1012.
24. J. James and P. Stewart MOPAC: A semi empirical molecular orbital program, *J. Comput. Aid. Mol. Des.* **4** (1990) 1–103.
25. S. Wold, C. Albano, W. Dunn, U. Edlund, K. Esbensen, P. Geladi, S. Hellberg, E. Johansson, W. Lindberg and M. Sjosstrom, *Mathematics and Statistics in Chemistry*, in *Chemometrics* (Ed. B. Kowalski), Reidel, Dordrecht 1987, pp. 17.

S A Ž E T A K

3D-QSAR CoMFA/CoMSIA studije derivata 5-aril-2,2-dialkil-4-fenil--3(2*H*)-furanona, kao selektivnih COX-2 inhibitora

DEVENDRA SHARAD PUNTAMBEKAR, RAJANI GIRIDHAR i MANGE RAM YADAV

Komparativna molekularna analiza polja (CoMFA) i komparativna analiza sličnosti molekularnih indeksa (CoMSIA) provedena je na seriji derivata 5-aril-2,2-dialkil-4-fenil-3(2*H*)-furanona kao selektivnih inhibitora ciklooksigenaze-2 (COX-2). Superimpozicija molekularnih liganada na uzorak strukture provedena je prilagodbom korijena usrednjenih kvadratnih udaljenosti temeljenih na udaljenostima atoma i na obliku molekule i metodom poravnavanja unutar skupa podataka. Uklanjanjem tri spoja koji jako odstupaju iz početnog skupa od 49 molekula povećala se točnost predviđanja modela. Postavljen je statistički značajan model od 36 molekula, koji je provjeren na dodatnom skupu od deset spojeva. Prilagodba korijena usrednjenih kvadratnih udaljenosti temeljenih na udaljenostima atoma i na obliku molekule dala je najbolji CoMFA model sa 6 komponenata koji ima R^2_{cv} = 0,664 (križno provjereni kvadrat koeficijenta korelacije), R^2 = 0,916, F vrijednost 47,341, kod kojega je standardna pogreška predviđanja 0,360 i standardna pogreška procjene 0,180. Za CoMSIA model sa 4 komponente dobiveni su parametri R^2_{cv} = 0,777, R^2 = 0,905, F vrijednost 66,322, standardna pogreška predviđanja 0,282 i standardna pogreška procjene 0,185. Iz mapa obrisa dobivenih 3D-QSAR studijom procijenjeni su trendovi aktivnosti za analizirane molekule. Rezultati ukazuju da

sterički, elektrostatski, hidrofobni (lipofilni) supstituenti i oni koji mogu tvoriti vodikovu vezu imaju značajnu ulogu u inhibitornom djelovanju na COX-2 i selektivnost spojeva. Podaci dobiveni ovom studijom pomoći će u dizajniranju novih, snažnih i selektivnih COX-2 inhibitora.

Ključne riječi: 3D-QSAR, CoMFA, CoMSIA, inhibitori ciklooksigenaze-2, protuupalne tvari

Pharmacy Department, Faculty of Technology and Engineering, Kalabhavan, The M. S. University of Baroda, Vadodara-390001, India